Cancer Letters 443 (2019) 80–90

Contents lists available at ScienceDirect

Cancer Letters

journal homepage: www.elsevier.com/locate/canlet

Original Articles

Inhibition of tankyrase by a novel small molecule significantly attenuates prostate cancer cell proliferation

Honglin Cheng[a], Xin Li[a], Chuanlin Wang[a], Yujie Chen[a], Sijiang Li[a], Jincai Tan[a], Bing Tan[b], Yunfeng He[a,*]

[a] Department of Urology, The First Affiliated Hospital, Chongqing Medical University, Chongqing, 400016, China
[b] Department of Functional Genomics and Cancer, Institute of Genetics and Molecular and Cellular Biology (IGBMC), CNRS UMR 7104, INSERM U 964, The University of Strasbourg, 1 rue Laurent Fries, 67404, Illkirch, France

ARTICLE INFO

Keywords:
TNKS inhibitor
Wnt signaling
Protein-protein interaction
Prostate cancer

ABSTRACT

Tankyrase (TNKS) is a crucial mediator of Wnt signal transduction and has been recognized as a novel molecular target for Wnt-pathway dependent cancer. TNKS is stabilized by the ubiquitin-specific protease 25 (USP25). The effect of disruption of the interaction between TNKS and USP25 by small molecules on prostate cancer proliferation is unknown. In this study we conducted a hierarchical virtual screening with more than 200,000 compounds on the characterized structures of the USP25/TNKS-ARC5 protein complex. In silico analysis and in vitro validation revealed that a small molecule, called C44, binds to the protein-protein interaction (PPI) interface of TNKS and USP25. We show that C44 disrupts the interaction between TNKS and USP25 leading to a higher half-life of AXIN and the breakdown of < beta > -catenin protein. We also show that the selective inhibition of the TNKS-USP25 interaction by C44 significantly reduces proliferation of prostate cancer cells in vitro and in vivo. Our study reveals a new PPI inhibitor that lowers the stability of TNKS protein and inhibits Wnt pathway signaling. C44 is a promising new drug for the treatment of Wnt-pathway dependent prostate cancer.

1. Introduction

Prostate cancer is the most commonly diagnosed cancer and the fifth most prevalent disease condition among men in the world [1]. For non-advanced prostate cancer, prostatectomy remains a primary treatment option. However, for advanced prostate cancer, which is commonly known as castration resistant prostate cancer, prostatectomy generally fails as well as androgen deprivation therapies [2]. In addition to endocrine therapy, chemotherapy has become a major clinical therapeutic option for advanced prostate cancer to improve prognosis [3].

A large number of studies have shown that the Wnt/β-catenin pathway is crucial for the development and progression of prostate cancer [4–6]. The Wnt signaling pathway is involved in multiple developmental events during embryogenesis and has been implicated in adult tissue homeostasis and tumorigenesis [7]. Mutations that activate Wnt signaling have been reported in approximately 5% of prostate cancer [8,9]. Thus, developing inhibitors of the Wnt/β-catenin pathway as a novel anti-cancer therapy has been of great interest in the cancer field. However, despite of intensive efforts, anti-Wnt-based therapies remain as a great challenge due to the dearth of kinases and other druggable targets known to be present in the Wnt pathway [10].

Tankyrase (TNKS), member of poly(ADP-ribose)polymerase (PARP) family, is crucial mediator of Wnt signal transduction and have been recognized as promising potential therapeutic targets for developing anti-Wnt therapy [10,11]. TNKS-mediated poly(ADP-ribosyl)ation and consequent degradation of AXIN drives Wnt signaling [12]. Thus, catalytic inhibitors of TNKS have been developed by several major pharmaceutical companies with the goal to dampen Wnt signaling in cancer cells [10]. However, TNKS may be able to act as scaffolds to promote Wnt signaling independently of their PARP activity [13]. Thus, inhibition of the catalytic activity of TNKS may not be adequate for suppressing Wnt activity in cells with high levels of TNKS. Moreover, treatment of TNKS inhibitors on cancer cells may lead to increases in the level of TNKS and thereby exacerbate TNKS polymerization to induce drug resistance. Therefore, new avenues may be needed to target TNKS for developing inhibitors of Wnt signaling as anti-cancer therapy.

Currently all the TNKS inhibitors are targeting the donor NAD^+ binding site. Two other druggable sites exist on TNKS, namely the acceptor site and the ankyrin repeats [11]. TNKS is stabilized by the ubiquitin-specific protease 25 (USP25)[14]. Disrupting the interaction between USP25 and TNKS promotes the degradation of TNKS and

* Corresponding author.
E-mail address: hyf028@126.com (Y. He).

https://doi.org/10.1016/j.canlet.2018.11.013
Received 21 August 2018; Received in revised form 8 November 2018; Accepted 9 November 2018

Abbreviations

TNKS	Tankyrase
USP25	ubiquitin-specific protease 25
PPI	protein-protein interaction
PARP	poly(ADP-ribose)polymerase
ITC	Isothermal Titration Calorimetry
PBS	phosphate-buffered saline
DMSO	dimethyl sulfoxide
IPTG	isopropyl-beta-D-thiogalactopyranosid
FBS	fetal bovine serum
GST	Glutathione S-transferase
EDTA	ethylenediaminetetraacetic acid
SDS-PAGE	sodium dodecyl sulfate–polyacrylamide gel electrophoresis
PVDF	polyvinylidene difluoride
STF	Super-Topflash
ARCs	ankyrin repeat clusters
EC50	half maximal effective concentration
YAP	Yes-associated Protein

consequent stabilization of AXIN to antagonize Wnt signaling [14]. The interaction of USP25 with TNKS is defined by a seven-amino-acid peptide [14], suggesting the possibility of identifying small molecule mimetics to disrupt this interaction as a novel therapeutic approach for the treatment of Wnt-related cancers, including prostate cancer [9]. Moreover, the interaction of ankyrin repeats in TNKS with USP25 offers a novel avenue for selectively targeting TNKS, as ankyrin repeats are not present in other members of PARP family [11].

Protein-protein interactions (PPIs) represent important and promising therapeutic targets that are associated with the regulation of various molecular pathways, particularly in cancer [15]. Thus, small molecules that inhibit PPIs have potential as therapeutic medicines themselves and also as useful experimental tools to elucidate pathological mechanisms. Although it is considered as challenging to identify small molecules that modulate PPIs, several reports provide encouraging evidence for finding such compounds [16,17]. In this study we used virtual screening strategy to search for novel small molecules targeting the protein-protein interaction interface of TNKS and USP25. We present an organic molecule that can prolong the halflife of AXIN and promote β-catenin degradation through promoting the degradation of TNKS by disrupting the interaction between TNKS and USP25. We show that the selective inhibition of TNKS-USP25 interaction by small molecular effectively reduces prostate cancer cell proliferation and significantly attenuates prostate cancer tumor growth in xenograft mice models. Our study uncovers a novel PPI inhibitor that decreases TNKS protein stability and inhibits Wnt pathway signaling, and its therapeutic exploitation holds promise for treating Wnt-pathway dependent prostate cancers.

2. Materials and methods

2.1. Virtual screening for TNKS-binding small molecules

A hierarchical virtual-screening strategy was based on characterized structures and the established mechanism [14]. DOCK4.0 was used for the initial screening on the Specs database, which contains more than 200,000 commercially available compounds. The TNKS crystal structure (PDB entry 5GP7) was used as the docking receptor and residues in the USP25-TNKS protein-protein interaction interface were defined as the binding site. A standard DOCK scoring function was used to rank the result list and the top-ranked 10,115 candidates were rescored by the CSCORE (consensus score) module of SYBYL 6.8 (Tripos Inc.). CSCORE combines multiple types of scoring functions, including FlexX, Dock, Gold, ChemScore and Potential Mean Force scoring schemes to produce a consensus to evaluate ligand-receptor interactions.

Compounds that had a consensus score of four or five or that were ranked in the top 10% by at least four out of five scoring functions were evaluated further by Autodock 4.0 [35]. Based on an empirical binding free energy estimated by Autodock 4.0, 301 compounds with the highest estimated binding affinity were chosen, and then structurally clustered to 50 clusters based on their two-dimensional (2D) molecular fingerprints using the Cluster Molecules module in Pipeline Pilot 7.5 (Scitegic, Inc.). To ensure the structural diversity of the selected compounds, two to three compounds with good drug-like properties (molecular weight < 500, log P < 5 and polar surface area < 140 Å) were selected from each cluster. Finally, 201 compounds in total were selected and purchased for the first round of biochemical assay described below. Based on the structures of the four active compounds identified by the first-round biochemical assay, a 2D similarity search and scaffold hopping were conducted using FP2 and SHAFTS methods implemented in the ChemMapper web server [36]. After water-solubility prediction and structural clustering of the 4 newly screened hits using Solubility and Cluster Molecules modules implemented in Pipeline Pilot 7.5, 61 structurally diverse candidates were purchased for the final biochemical assay.

2.2. Fluorescence polarization assay

USP25 C-terminal peptide (RTPADGR) was labelled with FITC (Molecular Probes) and purified by high-performance liquid chromatography. For the initial screening assays, 500 nM labelled peptide and 4.73 μM TNKS (178–957) protein mixed with phosphate-buffered saline (PBS), pH 7.4, were added to 96-well black plates. Small molecules, 10 μM in dimethyl sulfoxide (DMSO), were transferred by using plastic 96-pin arrays (Genetix). The plates were incubated for 1 h at 25 °C, and FP values were determined with an Analyst plate reader (LJL Biosystems). Kd and Ki determinations were performed as described previously [37] with a GraphPad Prism software package (GraphPad).

2.3. Protein expression and purification

The *E. coli* strain BL21 was transformed with pET28a-TNKS (178–957), cultured in lysogeny broth (LB) medium containing 50 mg/mL kanamycin at 37 °C to an absorbance of 0.6 at 600 nm, and induced with 1 mM isopropyl-beta-D-thiogalactopyranosid (IPTG) for 16 h at 16 °C before being harvested by centrifugation. The cell pellets were suspended in lysis buffer (10 mM Tris, pH 7.5, 200 mM NaCl, 1 mM DTT) and disrupted by sonication. After centrifugation, the supernatant was applied to a NiNTA column and proteins were eluted with elution buffer (10 mM Tris, pH 7.5, 200 mM NaCl, 1 mM DTT, and 400 mM Imidazole). The 6-His-tag was removed by digestion with thrombin. The samples were exchanged and further purified with the buffer using size-exclusion chromatography (S200 Sephacryl column, GE) in 50 Mm HEPES, 200 mM NaCl and 1 mM DTT. Fractions containing the protein were analyzed using SDS-PAGE and fractions showing a single band corresponding to the expected molecular weight were pooled, resulting in $> 95\%$ pure protein samples.

2.4. Isothermal Titration Calorimetry assay

Isothermal Titration Calorimetry (ITC) experiments were performed on an ITC200 or PEAQ-ITC machine (Malvern Instruments Ltd.) at 25 °C. The titration data were analyzed using the program Origin 7.0 from MicroCal and fitted using the one-site binding model. Analytic size exclusion chromatography experiments were performed on a Superdex 200 Increase 10/300 column (GE Healthcare). All proteins for these

assays were in the buffer containing 20 mM Tris (pH 7.5), 100 mM NaCl, and 1 mM DTT.

2.5. Compounds stock

All compounds are purchased from Shanghai Institute of Materia Medica. All compounds are soluble in DMSO and stock solutions of 50 mM were made before dilution with water in various assays. The concentration of DMSO is less to 5% for all in vitro assay buffers.

2.6. Cell culture, antibodies and reagents

HEK293T cells were cultured in DMEM (Gibco) with 10% (vol/vol) fetal bovine serum (FBS) (Gibco) and 1% penicillin/streptomycin. The prostate cancer cell line (PC-3 and LNCaP) were maintained in RPMI1640 supplemented with 10% (vol/vol) FBS, 1% penicillin/streptomycin. Cells were grown in a 37 °C humidified incubator containing 5% CO2. All the cell lines were purchased from American Tissue Culture Collection.

The commercial antibodies used for western blotting analysis include the following: anti-USP25 (ab187156, 1:1000 dilution) was from Abcam, anti-TNKS1/2 (sc-8337, 1:1000 dilution) was from Santa Cruz Biotechnology, anti-AXIN1 (#2087, 1:1000 dilution), anti-β-catenin (#9562, 1:1000 dilution), anti-AXIN2 (#2151, 1:1000 dilution) and anti-Flag (#2368, 1:1000 dilution) were from Cell Signaling Technology. Anti-Myc (16286-1-AP, 1:1000 dilution) and anti-HA (51064-2-AP, 1:1000 dilution) were from Proteintech. Anti-Tubulin (PM054, 1: 10000 dilution) was from MBL. XAV-939 (S1180) and MG132 (S2619) were from Selleckchem.

2.7. GST-WWE pull down assay

For Glutathione S-transferase (GST) pull downs, GST-WWE beads were generated as described previously [38]. HEK293T cells were treated as indicated, then washed once with cold 1 × PBS and lysed in lysis buffer (50 mM Tris-HCl [pH 8.0], 100 mM NaCl, 1% NP-40, 10% glycerol, 1.5 mM ethylenediaminetetraacetic acid (EDTA) [pH 8.0]) supplemented with 1 μM of the poly(ADP-ribose) glycohydrolase inhibitor ADP-HDP (Enzo Life Sciences), and protease and phosphatase inhibitor cocktail (1:100, Thermo Scientific). Lysates were incubated with GST-WWE beads overnight at 4 °C. Following incubation, beads were washed four times in wash buffer (50 mM Tris-HCl [pH 8.0], 150 mM NaCl, 1% NP-40, 10% Glycerol, 1.5 mM EDTA [pH 8.0]) supplemented with 1 μM ADP-HPD and protease and phosphatase inhibitor cocktail (1:100). Bound materials were eluted with 2 × sample buffer and resolved by sodium dodecyl sulfate–polyacrylamide gel electrophoresis (SDS-PAGE), transferred to polyvinylidene difluoride (PVDF) membranes and blotted with the indicated antibodies.

2.8. In vitro compound competition assay

Flag-USP25 or HA-AXIN1 was transfected into HEK293T cells for 24 h, then washed once with cold 1 × PBS and lysed in lysis buffer (50 mM Tris-HCl [pH 8.0], 100 mM NaCl, 1% NP-40, 10% glycerol, 1.5 mM EDTA [pH 8.0]) supplemented with protease and phosphatase inhibitor cocktail. Lysates were incubated with anti-Flag beads (Flag-USP25) or anti-HA beads (HA-AXIN1) (Sigma) for 4 h at 4 °C. Beads were washed three times in wash buffer (50 mM Tris-HCl [pH 8.0], 150 mM NaCl, 1% NP-40, 10% Glycerol, and 1.5 mM EDTA [pH 8.0]). Then the compound with indicated concentration was added to the beads. Following incubation in ice for 1 h, beads were washed four times in wash buffer. The remain bound materials were eluted with 2 × sample buffer and resolved by SDS-PAGE, transferred to PVDF membranes and blotted with the indicated antibodies.

2.9. Luciferase reporter assay

HEK293T cells were transfected with Super-Topflash (STF) reporter plasmid and an internal reference plasmid for 4–6 h, then cells were activated with Wnt3a conditioned medium (1:1) for another 12–18 h. STF luciferase assays were performed by using the Dual Luciferase Assay kit (Promega) according to the manufacturer's instructions.

2.10. Ni-NTA pulldown analysis

HEK293T cells were transfected with relevant expressing vectors for 24 h, cells were then lysed in 8 M urea. Equal amounts of cell extracts (1 mg) and 40 μl Ni-NTA-agarose beads (Qiagen) were incubated overnight at room temperature. Precipitates were washed 3 times with the same buffer and subjected to SDS-PAGE.

2.11. Cell proliferation and colony formation assays

For proliferation assays, cells were seeded at a concentration of 1000 cells/well in flat bottom 96-well microplates. Cell proliferation was measured at the indicated time using Cell Counting Kit-8 (#B34302, Biotool), according to the manufacturer's instructions. For colony formation assays, cells were seeded in low serum growth medium (0.5% FBS) at 1000 cells per well into six-well plates in triplicates. Medium was replenished every 3 d, and cells were incubated for 14 d. Resulting colonies were fixed with 4% PFA and stained by a solution of 2 mg/ml crystal violet in PBS. The numbers of colonies were counted.

2.12. CRISPR-Cas9 mediated gene knockout

Usp25 was knocked out from HEK293T cells using the CRISPR/Cas9 system, with a guide RNA spanning exon 2. The guide RNA was individually cloned into the pX330 vector and transfected into HEK293T cells. Transfected cells were sorted by fluorescence-activated cell sorting using green fluorescent protein. Single colonies were screened using western blot and DNA sequencing to confirm the loss of USP25 protein expression. The following target site sequences, transduced via pX330, were used: TCAAGGCTTGCTGTAGTATC (minus strand).

2.13. Xenograft studies

Nude mice (nu/nu, male 6–8 week old, Charles River Laboratories) were subcutaneously injected with 10×10^6 PC-3 cells on their right flanks. For evaluation of C44 using xenograft mice, the molecule was administered daily by i.p. injection with a dose of 100 mg kg^{-1} from 6 days after subcutaneous injection of PC-3 cells on the right flank of each mouse. Tumor growth was recorded by measurement of two perpendicular diameters of the tumors over a 3-week period using the formula $4\pi/3 \times (\text{width}/2)^2 \times (\text{length}/2)$. The tumors were harvested and weighed at the experimental endpoint, and the masses of tumors (g) treated with vehicle control (DMSO) and C44 was compared by a two-tailed unpaired Student's test. Use of nude mice were approved by the Review Board of Chongqing Medical University (Chongqing, China). The animal care and use program complied with the 1996 Guide for the Care and Use of Laboratory Animals.

2.14. Statistical analysis

Statistical analysis and graphical presentation were done using GraphPad Prism 5.0. Data shown are from one representative experiment of multiple independent experiments and are given as mean ± SEM. $P < 0.05$ was considered to indicate statistical significance.

3. Results

3.1. Developing small molecules that specifically inhibit TNKS-USP25 interaction

Since modulating the interaction of USP25 with TNKS provides an opportunity to promote the degradation of TNKS rather than inhibiting their enzymatic activities, we set up to develop organic small molecules that inhibits the interaction of TNKS and USP25. Since the N-terminal part of TNKS is consist of five ankyrin repeat clusters (ARCs), of which, ARC5 showed stronger binding to USP25 than other ARCs [14], we aimed to find small molecules that may bind to ARC5 and block the

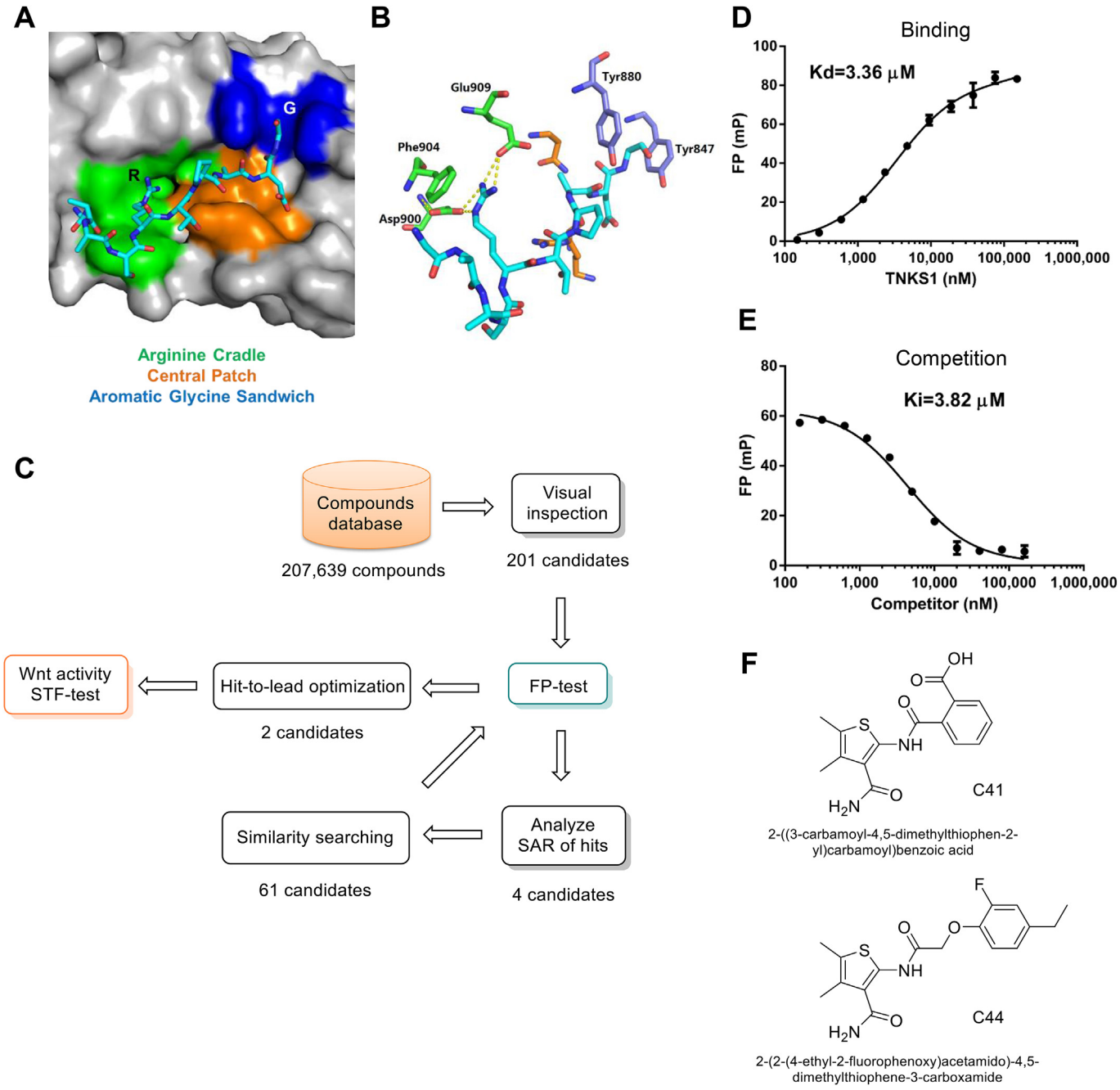

Fig. 1. Developing small molecules that specifically inhibit TNKS-USP25 interaction. (**A** and **B**) The electrostatic surface shows the "arginine cradle" and "aromatic glycine sandwich" of TNKS-ARC5, which accommodate two charged residues (R1049 and G1054) of USP25. The "arginine cradle" is colored in green, "aromatic glycine sandwich" is colored in blue, while the central patch is colored in orange (A). In the crystal structure of the complex formed by TNKS1 ARC5 (residues 799–957) and the last 10 residues of USP25 (residues 1046–1055), the hydrogen bonds that formed in the "arginine cradle" of TNKS-ARC5 with USP25 residues are shown as dashed lines (B). PDB accession: 5GP7. (**C**) A hierarchical docking strategy was adopted: DOCK4.0 was used to screen the Specs database, which contains more than 200,000 compounds. Out of this screen, and based on their structural features, physical chemistry properties and drug-like characteristics, 201 compounds were selected for further bioactivity testing with four hits discovered. With SAR analysis of these four hits, 61 candidates were subjected to similarity searching, resulting the two final hits. (**D**) Titration of USP25 C-terminal peptide (RTPADGR) labelled with FITC (500 nM) with increasing amounts of TNKS (178–957) protein. Binding of the peptide is accompanied by an increase in polarization. mP, millipolarization. 3 replicates. (**E**) Competition of the fluorescently labelled RTPADGR peptide ('tracer', 500 nM) with increasing amounts of the unlabeled Trx-RTPADGR peptide ('competitor') for binding to TNKS(178–957) protein (4.73 μM). 3 replicates. (**F**) The structures and chemical names of the compounds selected through the screening.

interaction of USP25 and TNKS. We performed a hierarchical virtual screening strategy based on characterized structures of USP25/TNKS-ARC5 complex [14].

In the structures of USP25/TNKS complex, the C-term of USP25 adopts an extended conformation and binds to the central concave side of TNKS [14] (Fig. 1A). The positively charged side chain of R1049 of USP25 is recognized by a highly negatively charged pocket ("arginine cradle"), where four residues from TNKS1 contribute extensive interactions: The side chains of E909 and D900 form two salt bridges with the side chain of R1049, whereas F904 establishes a cation-π interaction with the guanidinium group of R1049 (Fig. 1B). Based on this binding model of "arginine cradle" between USP25 and TNKS, we used DOCK4.0 [18] to screen the Specs database, which contains more than 200,000 compounds, to find small molecules that may fit this "arginine cradle". Out of this screen, and based on the structural features, physical chemistry properties and drug-like characteristics, 201 compounds were selected for more bioactivity testing (Fig. 1C).

To validate small molecules identified in the virtual screening, we developed a fluorescence polarization (FP)-based binding competition assay [19] to measure these small molecules' binding to TNKS. We envisioned that a small molecule that specifically binds at the interface would inhibit the formation of the complex between TNKS and USP25, which would lead to a decreased FP value. First, we used the C-terminal peptide of USP25 as a probe peptide, which is labelled with fluorescein isothiocyanate (FITC). We validated the binding of this probe peptide to TNKS and obtained the similar dissociation constant as reported (Kd = 3.36 μM) (Fig. 1D). This FP-based binding competition assay was further confirmed by using an unlabeled C-terminal peptide of USP25 to co-incubate with the probe peptide competing for the binding to TNKS. An inhibition constant (Ki = 3.82 μM) was obtained, which is consistent with the dissociation constant obtained (Fig. 1E). With this established FP-based binding competition assay, we found two compounds named C41 and C44, respectively, exhibiting strong inhibition of the USP25-TNKS interaction (Fig. 1F).

3.2. Docking model and binding of C44 to TNKS

The binding affinity of these two hits, C41 and C44, to TNKS is

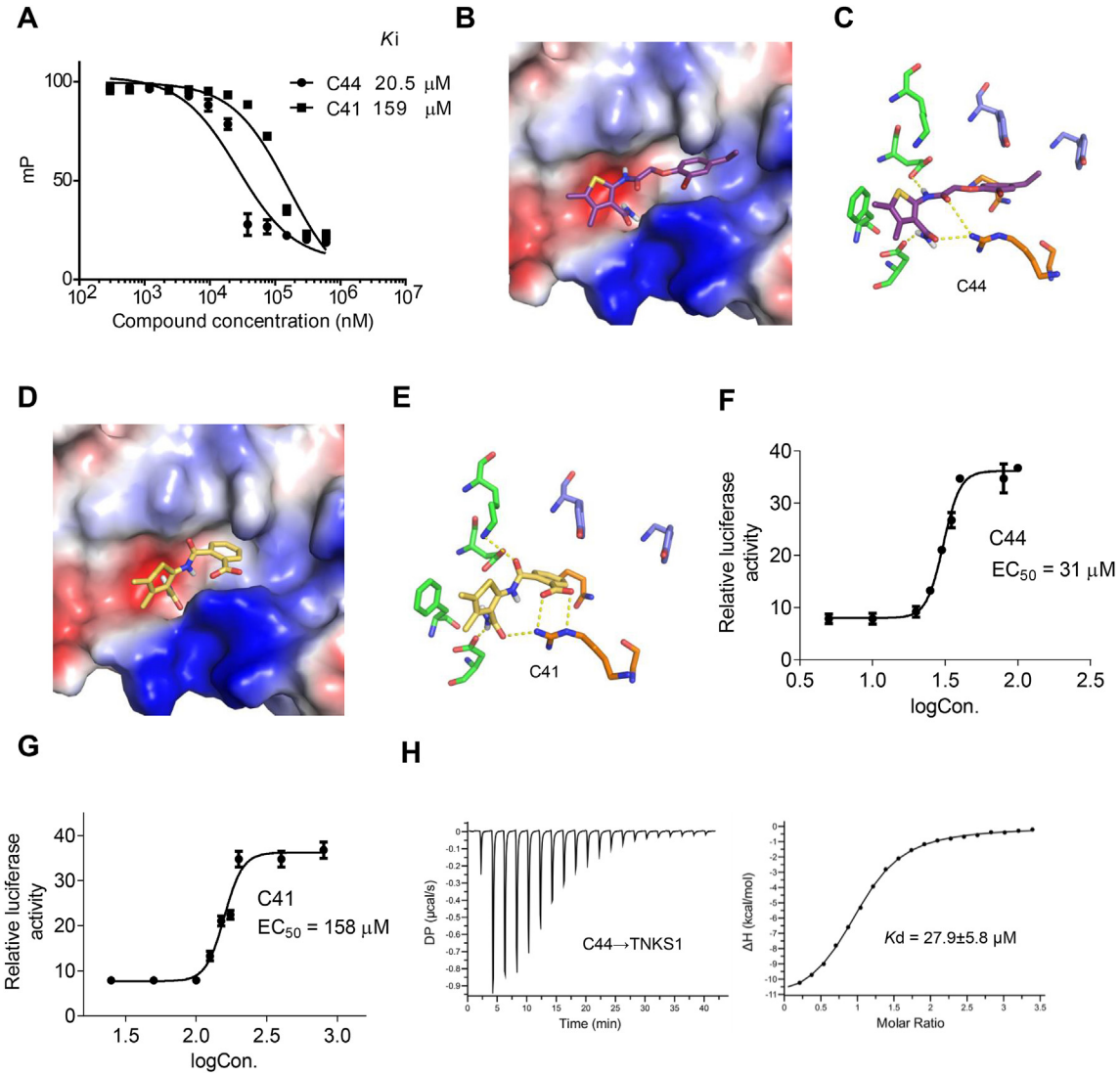

Fig. 2. Docking model and binding of C44 to TNKS. (**A**) Inhibition curves and Ki values of C44 and C41 (means ± SD) for the inhibition of TNKS(178–957)−USP25 interaction determined with FP titration assays are shown. (**B** and **C**) Surface representations that show C44 (purple) binding to TNKS1-ARC5 (PDB 5GP7) (B). The hydrogen bonds that formed between of TNKS-ARC5 and C44 are shown as dashed lines (C). (**D** and **E**) Surface representations that show C41 (yellow) binding to TNKS1-ARC5 (PDB 5GP7) (D). The hydrogen bonds that formed between of TNKS-ARC5 and C44 are shown as dashed lines (E). (**F** and **G**) Inhibition curves of C44 (F) and C41 (G) on Wnt pathway by STF Luciferase reporter assay. (**H**) ITC assay measuring the binding affinity between C44 and the ankyrin repeat region (residues 178–957) of TNKS. (For interpretation of the references to color in this figure legend, the reader is referred to the Web version of this article.)

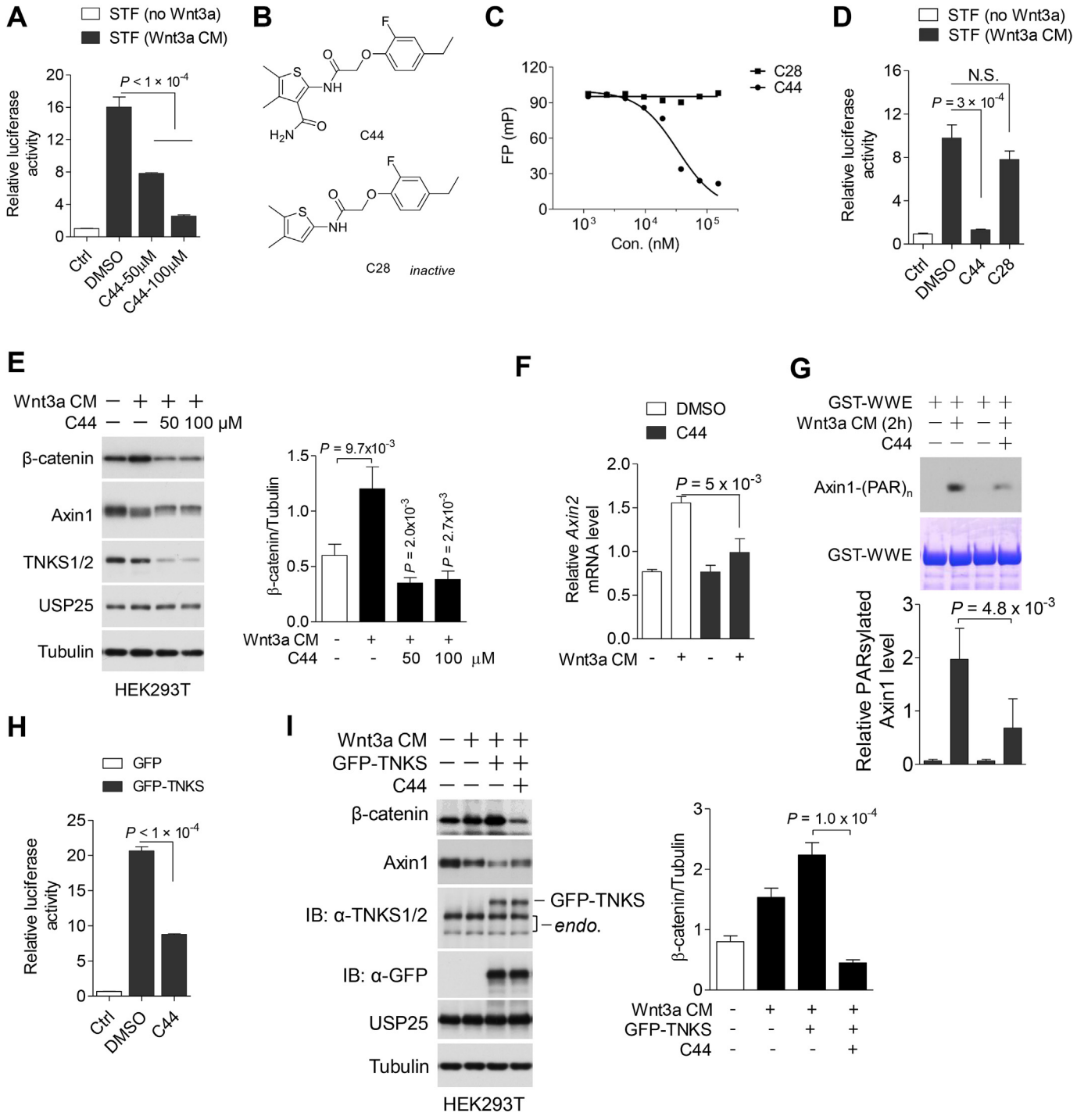

Fig. 3. C44 inhibits Wnt/β-catenin pathway. (**A**) C44 inhibits Wnt3a-induced Super-Topflash (STF) reporter in HEK293T cells in dose-dependent manner. Error bars denote the SD between three replicates. (**B**) The structure of C28, an inactive derivative of C44 that lacks the amide group. (**C**) C28 does not inhibit TNKS-USP25 interaction as determined by FP titration assay. (**D**) C28 does not inhibit Wnt3a-induced Super-Topflash (STF) reporter in HEK293T cells. Error bars denote the SD between three replicates. (**E**) C44 blocks Wnt3a-induced accumulation of β-catenin in HEK293T cells. HEK293T cells were pretreated with 50 μM C44 for 0.5 h then stimulated with or without Wnt3a conditioned medium (CM) for 12 h, and cells were harvested and then analyzed by Western blotting using the indicated antibodies. Ratios of β-catenin/Tubulin were calculated and are shown at the right. (**F**) C44 blocks Wnt3a-induced Axin2 up-regulation in HEK293T cells. (**G**) Immunoblot of lysates from HEK293T cells pretreated with 50 μM C44 for 0.5 h and then treated with Wnt3a CM for 2 h and then subjected to GST-WWE (Trp-Trp-Glu) pull-down. Treatment with Wnt3a CM increased the level of ADP-ribosylated Axin pulled down with GST-WWE. Ratios of PARsylated-Axin1/WWE were calculated and are shown at the right. (**H**) C44 inhibits TNKS overexpression-induced STF reporter. HEK293T cells expressing GFP-tagged TNKS or the GFP control were pretreated with 50 μM C44 for 0.5 h and then tested in the STF reported assay. Error bars denote the SD between three replicates. (**I**) C44 inhibits TNKS overexpression-induced accumulation of β-catenin in HEK293T cells. HEK293T cells expressing GFP-tagged were pretreated with 50 μM C44 for 0.5 h then treated with Wnt3a CM for 12 h, and cells were harvested and then analyzed by Western blotting using the indicated antibodies. Ratios of β-catenin/Tubulin were calculated and are shown at the right.

assessed by the inhibition constant determined by FP-based binding competition assay. As shown in Fig. 2A, C44 (Ki = 20.5 ± 13 μM) showed stronger binding than C41 (Ki = 159 ± 74 μM). We then built computational models to reveal the potential binding modes of C41 and C44 to ARC5 of TNKS, and these indicated that both C44 and C41 were bound with similar conformations to TNKS (Fig. 2B–E). The binding sites of the small molecules are located at the "arginine cradle" of TNKS (Fig. 2B and D), binding of the compounds would disrupt the protein-protein interactions of USP25 and TNKS. According to the model, the side chains of residues Glu909, Asp900 and Arg836 in TNKS form four hydrogen bonds with the heteroatoms of C44 (Fig. 2C). The side chains of residues Lys890, Asp900 and Arg836 in TNKS form five hydrogen bonds with the heteroatoms of C41 (Fig. 2E). In both models, F904 in TNKS1 establishes a cation-π interaction with the dimethylthiophene group of C44 and C41 (Fig. 2C and E).

We then characterized the inhibition effect of C44 and C41 by cellular assays, we determined the half maximal effective concentrations (EC50) of C44 and C41 using a well-established Wnt responsive SuperTopflash (STF) luciferase reporter assay [12] in HEK293T cells. The EC50s for C44 and C41 by STF assay are 31 μM and 158 μM, respectively (Fig. 2F and G). Taking into account both the FP-based binding competition assay and STF luciferase reporter assay, C44 was selected as the best candidate for our studies. C41 was later shown to be toxic in mice experiments, which led us to focus on C44.

To look for the direct binding of C44 and to TNKS, we performed isothermal titration calorimetry (ITC) assay, we found that the binding affinity of C44 revealed by ITC is 27.9 μM (Fig. 2H), which is similar to the inhibition constant obtained by FP-based binding competition

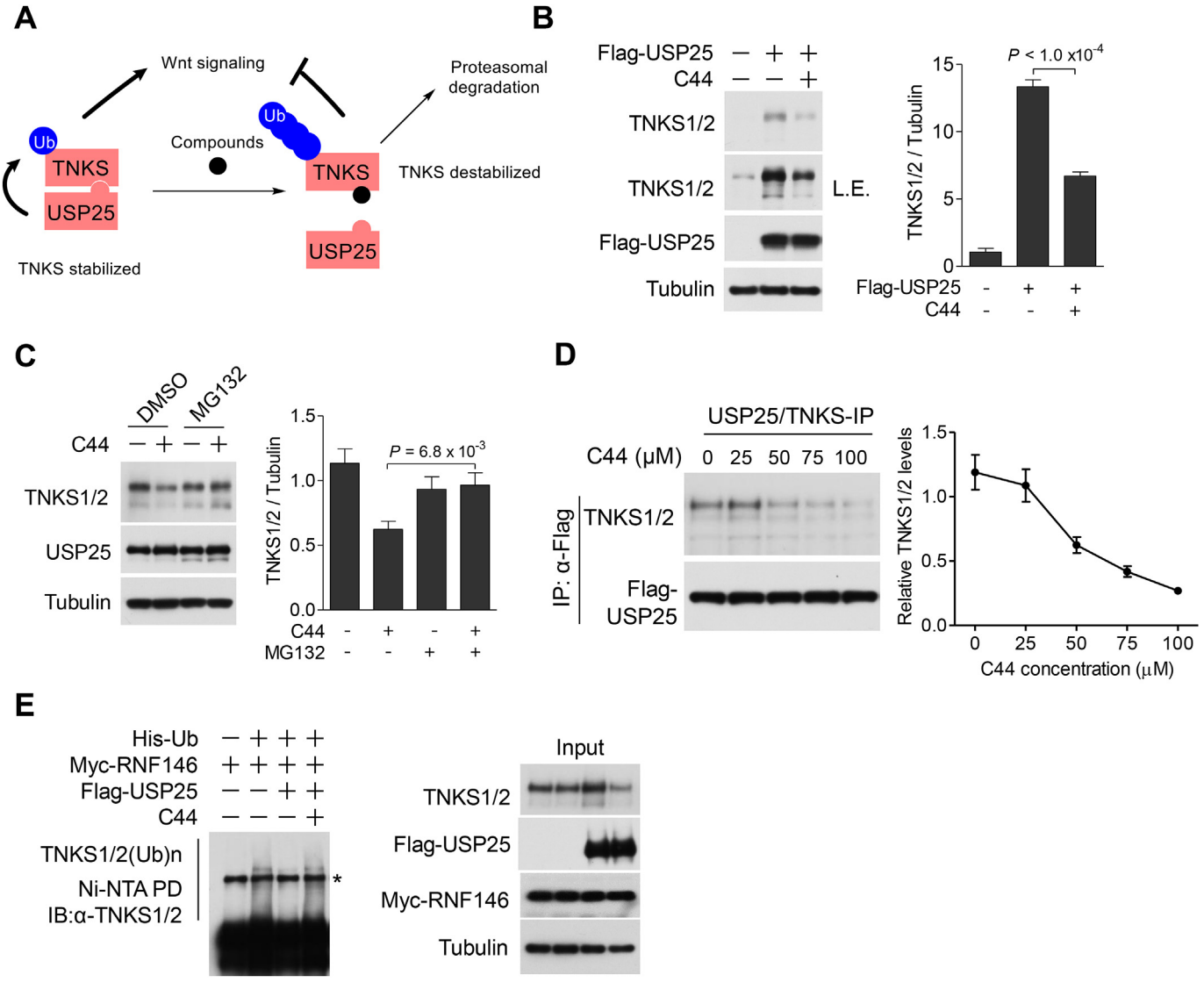

Fig. 4. C44 promotes TNKS degradation through disrupting TNKS-USP25 interaction. (**A**) A proposed working model for C44-induced TNKS destabilization and Wnt pathway inhibition by disrupting the interaction between TNKS and USP25. The deubiquitination of TNKS by USP25 leads to their stabilization by antagonizing ubiquitination. C44 disrupts TNKS-USP25 interaction and promotes the ubiquitination and degradation of TNKS. (**B**) C44 antagonizes USP25 overexpression-induced stabilization of TNKS. Flag-tagged USP25 was transfected into HEK293T cells for 4 h, then 50 μM C44 was added to the medium for another 8 h, and cells were harvested and then analyzed by Western blotting using the indicated antibodies. Ratios of TNKS/Tubulin were calculated and are shown at the right. (**C**) C44 promotes proteasomal degradation of TNKS. HEK293T cells were treated with 50 μM C44 for 6 h in the presence or absence of proteasome inhibitor MG132 (10 μM), and cells were harvested and then analyzed by Western blotting using the indicated antibodies. Ratios of TNKS/Tubulin were calculated and are shown at the right. (**D**) C44 inhibits TNKS-USP25 interaction in a dose-dependent manner as determined by in vitro compound competition assay. Quantification of TNKS remaining binding with USP25 was shown right. (**E**) C44 restores the ubiquitination of TNKS mediated by the E3 ligase RNF146 in USP25-overexpressed cells. HEK293T cells were transfected with the indicated constructs for 4 h, then treated with 50 μM C44 for another 8 h. The ubiquitination of TNKS was analyzed by Ni-NTA pull-down (PD) assay.

assay.

3.3. C44 inhibits Wnt/β-catenin pathway

We found that the treatment of C44 significantly reduced this Wnt-driven luciferase activity in a dose-dependent manner (Figs. 2F and 3A). In contrast, C28, an inactive derivative of C44 that lacks the amide group (Fig. 3B and C), did not significantly affect Wnt signaling as determined by the STF assay (Fig. 3D). Moreover, the Wnt3a-stimulated accumulation of β-catenin was strongly inhibited by C44 (Fig. 3E). Finally, C44 also inhibited the expression of the β-catenin target gene *AXIN2* (Fig. 3F).

It has been reported recently that TNKS-mediated PARsylation of AXIN not only controls its level but also allows PARsylated AXIN to directly promote Wnt signaling [12]. In order to detect whether C44 affects the levels of PARsylated AXIN in Wnt stimulation, we used a previously developed pull-down assay based on the ability of the Trp-Trp-Glu (WWE) domain of the RING-type E3 ubiquitin ligase RNF146 to bind to PARsylated proteins [20]. Within 2 h of Wnt3a exposure, the levels of PARsylated AXIN increased as reported previously, but this increase was notably reduced in C44-treated cells (Fig. 3G).

Since TNKS overexpression leads to the activation of Wnt signaling in Wnt3a-stimulated cells, we reasoned that C44 might also inhibit TNKS overexpression-induced Wnt signaling activation. To this end, GFP-tagged TNKS was introduced into HEK293T cells by lentivirus mediated infection, a dramatic increase of STF activity in TNKS-overexpressed cells was observed, which can be blocked by C44 (Fig. 3H). In addition, the Wnt3a-stmulated accumulation of β-catenin in TNKS-overexpressed cells was strongly inhibited by C44 (Fig. 3I). Collectively, these results suggest that C44 inhibits Wnt/β-catenin pathway.

3.4. C44 promotes TNKS degradation through disrupting TNKS-USP25 interaction

Since USP25 was found to stabilize TNKS [14], disrupting USP25-TNKS1 interaction by small molecular will promote the degradation of TNKS1 (Fig. 4A). While overexpression of USP25 increased TNKS protein levels as reported [14], treatment of C44 dramatically decreased TNKS levels in USP25-overexpressed cells (Fig. 4B). The effect of C44 on decreasing TNKS protein levels was also found in wild type cells (Fig. 4C). In addition, inhibiting the proteasome activity by a proteasome inhibitor MG132, restored the levels of TNKS in C44-treated cells (Fig. 4C), suggesting C44 promotes the proteasomal degradation of TNKS. To examine whether C44 blocks the interaction between TNKS and USP25, we performed an in vitro compound competition experiment, and showed that C44 blocks the interaction between USP25 and TNKS at 50 μM (Fig. 4D). Because TNKS was reported to be ubiquitinated by the E3 ligase RNF146 [21], and USP25 was found to deubiquitinate TNKS [14], we then examined whether C44 could restore the ubiquitination of TNKS in USP25-overexpressed cells by disrupting the binding between USP25 and TNKS. As shown in Fig. 4E, while USP25 inhibited the ubiquitination of TNKS mediated by RNF146, adding of C44 restored the ubiquitination of TNKS. Taken together, these results suggest that C44 promotes proteasomal degradation of TNKS by disrupting the interaction between TNKS and USP25.

3.5. C44 disrupts TNKS-AXIN1 interaction

Because the ankyrin repeat domain of TNKS was also required and sufficient for the interaction with AXIN [12,22], we reasoned that C44 may also disrupt the interaction between TNKS1 and AXIN (Fig. 5A). In order to exclude the effect of USP25, we assessed the functional consequences of disrupting the interaction between AXIN and TNKS in *Usp25*^{KO} HEK293T cells. Compared with wild type cells, Wnt3a slightly induced the activation of Wnt signaling in *Usp25*^{KO} cells as determined

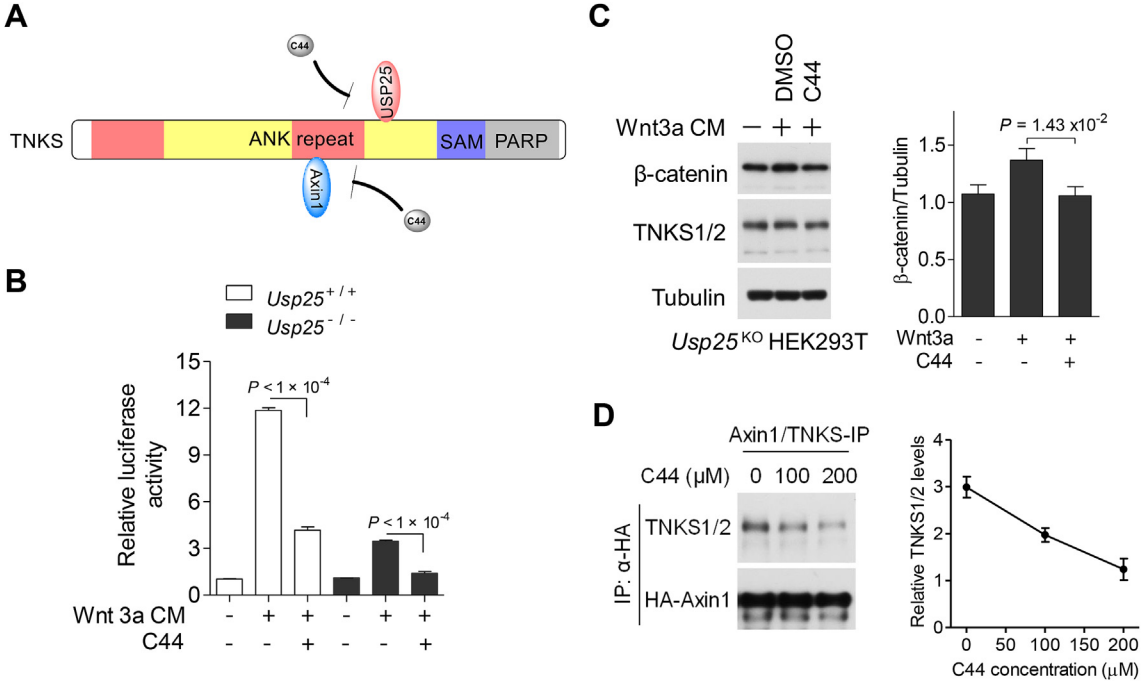

Fig. 5. C44 disrupts TNKS-AXIN1 interaction. (**A**) Illustration of C44 disrupting both TNKS-USP25 interaction and TNKS-AXIN1 interaction. Both USP25 and AINX1 binds to the ankyrin (ANK) repeats of TNKS. (**B**) C44 inhibits STF activity further in *Usp25*^{KO} HEK293T cells. (**C**) C44 blocks Wnt3a-induced accumulation of β-catenin in *Usp25*^{KO} HEK293T cells. *Usp25*^{KO} HEK293T cells were pretreated with 50 μM C44 for 0.5 h then stimulated with or without Wnt3a CM for 12 h, and cells were harvested and then analyzed by Western blotting using the indicated antibodies. Ratios of β-catenin/Tubulin were calculated and are shown at the right. (**D**) C44 inhibits TNKS-AXIN1 interaction in a dose-dependent manner as determined by in vitro compound competition assay. Quantification of TNKS remaining binding with AXIN1 was shown right.

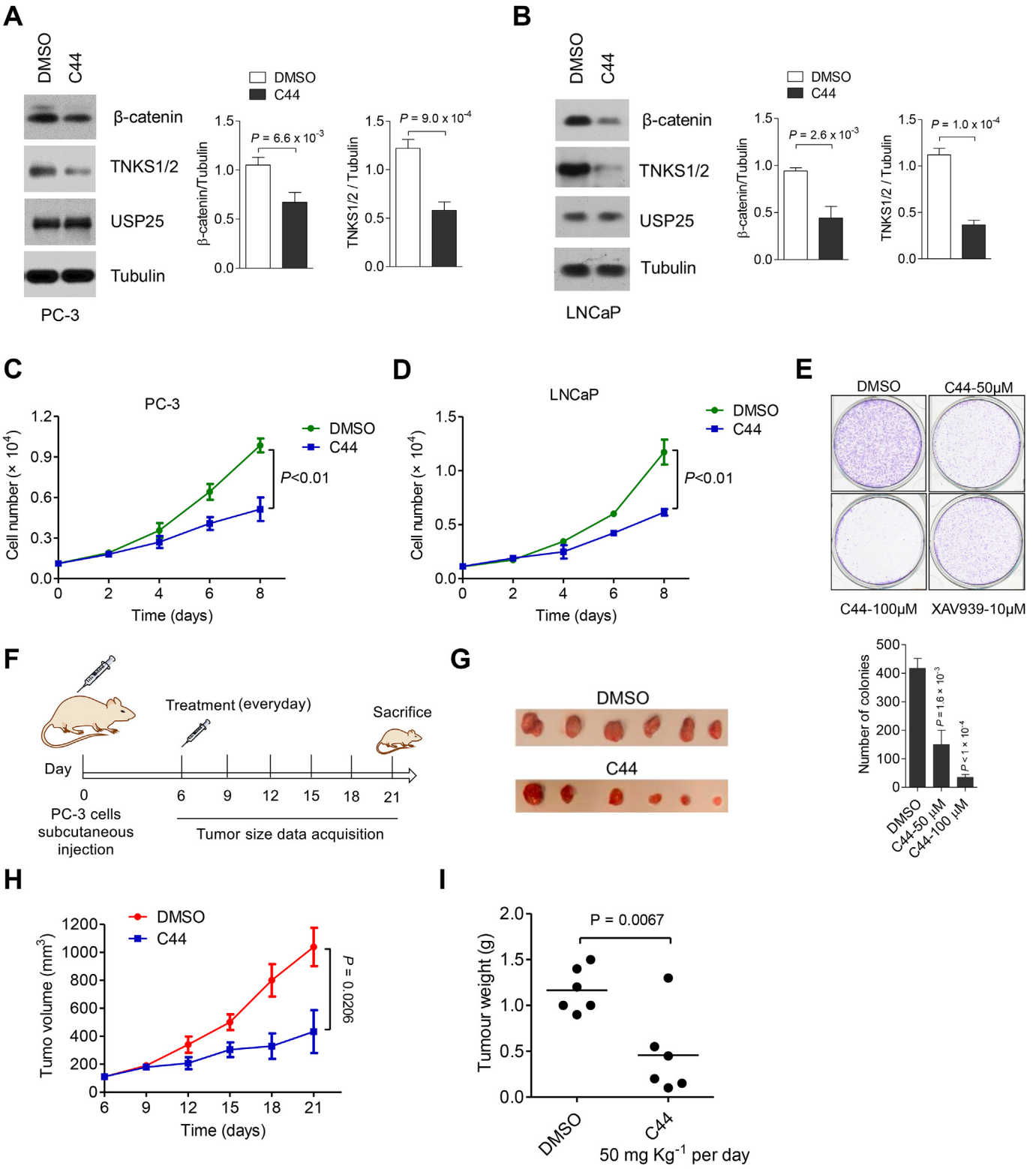

Fig. 6. C44 attenuates prostate cancer cell proliferation by inhibiting Wnt signaling. (**A,B**) C44 decreases the protein levels of TNKS and blocks accumulation of β-catenin in PC-3 cells(A) and LNCaP cells (B). PC-3 cells or LNCaP cells were treated with 50 μM C44 for 12 h, and cells were harvested and then analyzed by Western blotting using the indicated antibodies. Ratios of β-catenin/Tubulin and TNKS/Tubulin were calculated. (C–E) C44 inhibits the proliferation of PC-3 cells (C,E) and LNCaP cells (D), PC-3 cells or LNCaP cells treated with C44 were examined to determine their rate of cell proliferation. Cell proliferation assay was performed (C, D). Error bars denote the SD between three replicates. Colony formation assay was performed (E). Colonies viable after 2 wks were counted and analyzed. n = 3. (F) Illustration of the experimental design. (G) Images of excised tumors on the 21st day. (H)Tumor volume was recorded as indicated in (F) and totally for 21 days. (I) Tumor weight in xenograft nude mice injected with PC-3 cells compared with the group of mice treated with C44 and the control group treated with vehicle control. Error bars, mean ± SEM, n = 3 biological replicates. P values were determined by a two-tailed Student's *t*-test.

by the STF assay, which can be furtherly inhibited by C44 (Fig. 5B). Moreover, the Wnt3a-stmulated accumulation of β-catenin in *Usp25*^{KO} cells was also inhibited by C44 (Fig. 5C). These results suggest that C44 functions through both USP25-dependent and -independent manners. To test if C44 indeed disrupts the interaction between TNKS and AXIN, we performed the in vitro compound competition experiment, and showed that C44 also blocked the interaction between AXIN and TNKS (Fig. 5D).

Taken together, our results suggest that C44 inhibits Wnt signaling by disrupting the interaction between TNKS and USP25 to promote TNKS degradation and the interaction between TNKS and AXIN to prevent TNKS/AXIN1 axis-mediated activation of Wnt signaling.

3.6. C44 attenuates prostate cancer cell proliferation by inhibiting Wnt signaling

Since the Wnt/β-catenin pathway is crucial for the development and progression of prostate cancer [9], we then evaluated the effect of C44 on the protein levels of β-catenin and TNKS on prostate cancer cells. Western blot analysis revealed a significant decrease of β-catenin as well as TNKS in prostate cancer PC-3 cells treated with C44 (Fig. 6A). We then examined the effect of C44 on the proliferation of PC-3 cells and found that cells treated with C44 proliferated considerably slower than control cells (Fig. 6B). Under low-serum growth conditions, treatment of C44 significantly inhibited colony formation of PC-3 cells (Fig. 6C). Taken together, these results support TNKS-USP25 interaction as the cellular targets of C44 in inhibiting prostate cancer cell proliferation.

To test the effect of C44 on tumor xenograft growth, we synthesized a large quantity of C44 for animal model work(see the Supplementary Information).The initial toxicity studies by the chronic injection of C44(50 mg kg^{-1} per day) into nude mice revealed that C44 did not result in significant alterations in complete blood-cell counts or in the hematopoietic properties of nude mice(Figure S5).Then nude mice were injected with PC-3 cells and treated with 50 mg kg^{-1} per day of C44 for 21 days(Fig. 6F).we found that treatment with C44 resulted in a significantly decreased tumor size compared with mice that received the vehicle control(Fig. 6G and H).The collected tumors from these mice were also weighed,and again the group treated with C44 resulted in the lightest tumors and the strongest inhibition effect(Fig. 6I).These data indicate that targeting TNKS-USP25 interaction by C44 can suppress prostate cancer tumor growth effectively.

4. Discussion

Since TNKS is stabilized by USP25, disrupting the interaction between TNKS and USP25 is known to decrease the stability of TNKS and promote AXIN1 stabilization and thus inhibit Wnt/β-catenin pathway [14]. The interaction of ankyrin repeats in TNKS with the C terminus of USP25 offers a novel avenue for selectively targeting TNKS, as ankyrin repeats are not present in other members of PARP family [10]. Modulating the interaction of USP25 with TNKS provides an opportunity to stabilize AXIN and inhibit Wnt/β-catenin pathway by promoting the degradation of TNKS rather than inhibiting their enzymatic activities. In the present study, we used virtual screening strategy to search for novel small molecules targeting the protein-protein interaction interface of TNKS and USP25. We developed a small molecule C44 that can disrupt the interaction between TNKS and USP25 and promote the destabilization of TNKS. We demonstrated that C44 could prolong the halflife of AXIN and promote β-catenin degradation and consequently inhibit Wnt/β-catenin pathway.

Wnt signaling is a critical pathway for regulating development and adult tissue homeostasis. However, aberrant activation of Wnt signaling will induce constitutively transcriptionally activation of proto-oncogenes related with cell proliferation and apoptosis [23]. Aberrant activation of Wnt/β-catenin signaling has been frequently identified in many tumor types including bone sarcoma [24], oral squamous cell carcinomas [25], colorectal cancer [26], as well as prostate cancer [27]. It has been illustrated that miR-744 and miR-182 promoted prostate cancer progression through aberrantly activating Wnt/β-catenin signaling [8,27]. Additionally, up-regulation of Wnt/β-catenin was found to be correlated with high Gleason score, hormone-refractory and metastatic prostate cancer status [28,29]. Therefore, the activity of the Wnt/β-catenin pathway needs to be regulated delicately to maintain its proper function during development and in adult tissue homeostasis. We showed that inhibiting Wnt/β-catenin pathway by C44 effectively reduces prostate cancer cell proliferation and significantly attenuates prostate cancer tumor growth in xenograft mice models. Since C44 is an inhibitor for Wnt/β-catenin pathway, we propose that C44 may exhibit inhibitory effect on other Wnt-dependent tumor types.

TNKS have been shown to be involved in three different oncogenic proteins/pathways, including Yes-associated Protein (YAP) [30], Akt [31] as well as Wnt signaling pathway [12]. Thus, modulating the interaction between USP25 and TNKS may have effects on additional oncogenic signaling pathways such as those mediated by YAP and Akt. Since C44 promotes degradation of TNKS, we propose that C44 may also regulate YAP and Akt pathways in certain tumor types. It has been shown that both YAP and Akt pathways are activated in prostate cancer [32,33], although we have multiple experiments to demonstrate both in vitro and in vivo effects of the inhibitor, we could not exclude the potential presence of YAP and Akt pathways that may work synergistically with the inhibition of Wnt pathway in prostate cancer.

A number of small molecule inhibitors have been developed that target Wnt signaling in cancer. The best known of these are porcupine inhibitors, which block Wnt secretion, TNKS inhibitors, which inhibit β-catenin-dependent Wnt signaling by stabilizing AXIN, and drugs that target β-catenin interactions with transcription factors [34]. From a drug discovery and development perspective, the reason that TNKS represents attractive therapeutic target is inhibitors of TNKS could have broad clinical utility as TNKS function is implicated in many other processes such as the regulation of telomere length, lung fibrogenesis and myelination [10]. However, currently all the TNKS inhibitors are targeting the donor NAD^+ binding site. The donor NAD^+ binding site is also exhibited in other members of PARP family, which reduced the selectivity of these TNKS inhibitors. Our study uncovers a novel PPI inhibitor that targeting ankyrin repeats of TNKS, since ankyrin repeats are not present in other members of PARP family, this PPI inhibitor greatly increased the specificity of TNKS inhibition. Although the IC50 of C44 is relatively high as protein-protein interactions are difficult to target, it can be used for proof-of-concept studies in cancer and other TNKS linked diseases. The inhibitor and strategy presented here should stimulate future research and developments towards this goal.

In summary, a novel small molecule targeting the protein-protein interaction (PPI) interface of TNKS and USP25 was developed in the study. The selective inhibition of TNKS-USP25 interaction by small molecular effectively reduces prostate cancer cell proliferation and significantly attenuates prostate cancer tumor growth in xenograft mice models. Our study uncovered a novel PPI inhibitor that decreases TNKS protein stability and inhibits Wnt pathway signaling could be a promising therapeutics for Wnt-pathway dependent prostate cancer.

Acknowledgements

This study was supported by the Chongqing Municipal Education Commission (KJ1500207) and Chongqing Municipal Science and Technology Commission (No.cstc2018jcyjAX0188).

Appendix A. Supplementary data

Supplementary data to this article can be found online at https://doi.org/10.1016/j.canlet.2018.11.013.

Conflicts of interest

The authors declare no conflict of interest.

References

[1] R. Siegel, J. Ma, Z. Zou, A. Jemal, Cancer statistics, Ca - Cancer J. Clin. 64 (1) (2014) 9–29, https://doi.org/10.3322/caac.21208.

[2] H.W. Yang, M.Y. Hua, H.L. Liu, R.Y. Tsai, C.K. Chuang, P.C. Chu, et al., Cooperative dual-activity targeted nanomedicine for specific and effective prostate cancer therapy, ACS Nano 6 (2) (2012) 1795–1805, https://doi.org/10.1021/nn2048526.

[3] I.F. Tannock, R. de Wit, W.R. Berry, J. Horti, A. Pluzanska, K.N. Chi, et al., Docetaxel plus prednisone or mitoxantrone plus prednisone for advanced prostate cancer, N. Engl. J. Med. 351 (15) (2004) 1502–1512.

[4] Z. Zhu, H. Zhang, F. Lang, G. Liu, D. Gao, B. Li, et al., Pin1 promotes prostate cancer cell proliferation and migration through activation of Wnt/β-catenin signaling, Clin. Transl. Oncol. 18 (8) (2016) 792–797, https://doi.org/10.1007/s12094-015-1431-7.

[5] H. Liu, J. Yin, H. Wang, G. Jiang, M. Deng, G. Zhang, et al., FOXO3a modulates WNT/β-catenin signaling and suppresses epithelial-to-mesenchymal transition in prostate cancer cells, Cell. Signal. 27 (3) (2015) 510–518, https://doi.org/10.1016/j.cellsig.2015.01.001.

[6] J. Li, A. Karki, K.B. Hodges, N. Ahmad, A. Zoubeidi, K. Strebhardt, et al., Cotargeting polo-like kinase 1 and the Wnt/β-catenin signaling pathway in castration-resistant prostate cancer, Mol. Cell Biol. 35 (24) (2015) 4185–4198, https://doi.org/10.1128/MCB.00825-15.

[7] F. Takahashi-Yanaga, T. Sasaguri, The Wnt/beta-catenin signaling pathway as a target in drug discovery, J. Pharmacol. Sci. 104 (4) (2007) 293–302.

[8] D. Wang, G. Lu, Y. Shao, D. Xu, MiR-182 promotes prostate cancer progression through activating Wnt/β-catenin signal pathway, Biomed. Pharmacother. 99 (2018) 334–339, https://doi.org/10.1016/j.biopha.2018.01.082.

[9] M. Katoh, M. Katoh, Molecular genetics and targeted therapy of WNT-related human diseases (review), Int. J. Mol. Med. 40 (3) (2017) 587–606, https://doi.org/10.3892/ijmm.2017.3071.

[10] J.L. Riffell, C.J. Lord, A. Ashworth, Tankyrase-targeted therapeutics: expanding opportunities in the PARP family, Nat. Rev. Drug Discov. 11 (12) (2012) 923–936, https://doi.org/10.1038/nrd3868.

[11] T. Haikarainen, S. Krauss, L. Lehtio, Tankyrases: structure, function and therapeutic implications in cancer, Curr. Pharmaceut. Des. 20 (41) (2014) 6472–6488.

[12] S.M. Huang, Y.M. Mishina, S. Liu, A. Cheung, F. Stegmeier, G.A. Michaud, et al., Tankyrase inhibition stabilizes axin and antagonizes Wnt signalling, Nature 461 (7264) (2009) 614–620, https://doi.org/10.1038/nature08356.

[13] L. Mariotti, C.M. Templeton, M. Ranes, P. Paracuellos, N. Cronin, F. Beuron, et al., Tankyrase requires SAM domain-dependent polymerization to support Wnt-β-catenin signaling, Mol. Cell. 63 (3) (2016) 498–513, https://doi.org/10.1016/j.molcel.2016.06.019.

[14] D. Xu, J. Liu, T. Fu, B. Shan, L. Qian, L. Pan, et al., USP25 regulates Wnt signaling by controlling the stability of tankyrases, Genes Dev. 31 (10) (2017) 1024–1035, https://doi.org/10.1101/gad.300889.117.

[15] J.A. Wells, C.L. McClendon, Reaching for high-hanging fruit in drug discovery at protein-protein interfaces, Nature 450 (7172) (2007) 1001–1009.

[16] M.R. Arkin, J.A. Wells, Small-molecule inhibitors of protein-protein interactions: progressing towards the dream, Nat. Rev. Drug Discov. 3 (4) (2004) 301–317.

[17] A.L. Hopkins, C.R. Groom, The druggable genome, Nat. Rev. Drug Discov. 1 (9) (2002) 727–730, https://doi.org/10.1038/nrd892.

[18] T.J. Ewing, S. Makino, A.G. Skillman, I.D. Kuntz, DOCK 4.0: search strategies for automated molecular docking of flexible molecule databases, J. Comput. Aided Mol. Des. 15 (5) (2001) 411–428.

[19] L. Yin, L.J. Stern, Measurement of peptide binding to MHC class II molecules by fluorescence polarization, Curr. Protoc. Im. 106 (2014) 1–12, https://doi.org/10.1002/0471142735.im0510s106.

[20] E. Yang, O. Tacchelly-Benites, Z. Wang, M.P. Randall, A. Tian, H. Benchabane, et al., Wnt pathway activation by ADP-ribosylation, Nat. Commun. 7 (2016) 11430, https://doi.org/10.1038/ncomms11430.

[21] M.G. Callow, H. Tran, L. Phu, T. Lau, J. Lee, W.N. Sandoval, et al., Ubiquitin ligase RNF146 regulates tankyrase and Axin to promote Wnt signaling, PLoS One 6 (7) (2011) e22595, , https://doi.org/10.1371/journal.pone.0022595.

[22] S. Morrone, Z. Cheng, R.T. Moon, F. Cong, W. Xu, Crystal structure of a Tankyrase-Axin complex and its implications for Axin turnover and Tankyrase substrate recruitment, Proc. Natl. Acad. Sci. U. S. A. 109 (5) (2012) 1500–1505, https://doi.org/10.1073/pnas.1116618109.

[23] K. Kawahara, T. Morishita, T. Nakamura, F. Hamada, K. Toyoshima, T. Akiyama, Down-regulation of beta-catenin by the colorectal tumor suppressor APC requires association with Axin and beta-catenin, J. Biol. Chem. 275 (12) (2000) 8369–8374.

[24] C. Chen, M. Zhao, A. Tian, X. Zhang, Z. Yao, X. Ma, Aberrant activation of Wnt/β-catenin signaling drives proliferation of bone sarcoma cells, Oncotarget 6 (19) (2015) 17570–17583.

[25] R. Vidya Priyadarsini, R. Senthil Murugan, S. Nagini, Aberrant activation of Wnt/β-catenin signaling pathway contributes to the sequential progression of DMBA-induced HBP carcinomas, Oral Oncol. 48 (1) (2012) 33–39, https://doi.org/10.1016/j.oraloncology.2011.08.008.

[26] B.S. Moon, W.J. Jeong, J. Park, T.I. Kim, S. Min do, K.Y. Choi, Role of oncogenic K-Ras in cancer stem cell activation by aberrant Wnt/β-catenin signaling, J. Natl. Cancer Inst. 106 (2) (2014) djt373, https://doi.org/10.1093/jnci/djt373.

[27] H. Guan, C. Liu, F. Fang, Y. Huang, T. Tao, Z. Ling, et al., MicroRNA-744 promotes prostate cancer progression through aberrantly activating Wnt/β-catenin signaling, Oncotarget 8 (9) (2017) 14693–14707, https://doi.org/10.18632/oncotarget.14711.

[28] Y. Sun, J. Campisi, C. Higano, T.M. Beer, P. Porter, I. Coleman, et al., Treatment-induced damage to the tumor microenvironment promotes prostate cancer therapy resistance through WNT16B, Nat. Med. 18 (9) (2012 Sep) 1359–1368.

[29] G. Chen, N. Shukeir, A. Potti, K. Sircar, A. Aprikian, D. Goltzman, et al., Up-regulation of Wnt-1 and beta-catenin production in patients with advanced metastatic prostate carcinoma: potential pathogenetic and prognostic implications, Cancer 101 (6) (2004) 1345–1356.

[30] W. Wang, N. Li, X. Li, M.K. Tran, X. Han, J. Chen, Tankyrase inhibitors target YAP by stabilizing angiomotin family proteins, Cell Rep. 13 (3) (2015) 524–532, https://doi.org/10.1016/j.celrep.2015.09.014.

[31] N. Li, Y. Zhang, X. Han, K. Liang, J. Wang, L. Feng, et al., Poly-ADP ribosylation of PTEN by tankyrases promotes PTEN degradation and tumor growth, Genes Dev. 29 (2) (2015) 157–170, https://doi.org/10.1101/gad.251785.114.

[32] D. Ready, K. Yagiz, P. Amin, Y. Yildiz, V. Funari, S. Bozdag, et al., Mapping the STK4/Hippo signaling network in prostate cancer cell, PLoS One 12 (9) (2017), https://doi.org/10.1371/journal.pone.0184590 e0184590.

[33] T. Jamaspishvili, D.M. Berman, A.E. Ross, H.I. Scher, A.M. De Marzo, J.A. Squire, et al., Clinical implications of PTEN loss in prostate cancer, Nat. Rev. Urol. 15 (4) (2018) 222–234, https://doi.org/10.1038/nrurol.2018.9.

[34] J.N. Anastas, R.T. Moon, WNT signalling pathways as therapeutic targets in cancer, Nat. Rev. Canc. 13 (1) (2013) 11–26, https://doi.org/10.1038/nrc3419.

[35] G.M. Morris, R. Huey, W. Lindstrom, M.F. Sanner, R.K. Belew, D.S. Goodsell, et al., AutoDock4 and AutoDockTools4: automated docking with selective receptor flexibility, J. Comput. Chem. 30 (16) (2009) 2785–2791, https://doi.org/10.1002/jcc.21256.

[36] J. Gong, C. Cai, X. Liu, X. Ku, H. Jiang, D. Gao, et al., ChemMapper: a versatile web server for exploring pharmacology and chemical structure association based on molecular 3D similarity method, Bioinformatics 29 (14) (2013) 1827–1829, https://doi.org/10.1093/bioinformatics/btt270.

[37] W.B. Dandliker, M.L. Hsu, J. Levin, B.R. Rao, Equilibrium and kinetic inhibition assays based upon fluorescence polarization, Methods Enzymol. 74 Pt (1981) 3–28.

[38] Y. Zhang, S. Liu, C. Mickanin, Y. Feng, O. Charlat, G.A. Michaud, et al., RNF146 is a poly(ADP-ribose)-directed E3 ligase that regulates axin degradation and Wnt signalling, Nat. Cell Biol. 13 (5) (2011) 623–629, https://doi.org/10.1038/ncb2222.